

## Research Article

# Synthesis of Nano-Flakes Ag•ZnO•Activated Carbon Composite from Rice Husk as A Photocatalyst under Solar Light

Anh-Tuan Vu<sup>1,\*</sup>, Thi Anh Tuyet Pham<sup>1</sup>, Thi Thuy Tran<sup>1</sup>, Xuan Truong Nguyen<sup>1</sup>,  
Thu Quynh Tran<sup>1</sup>, Quang Tung Tran<sup>1</sup>, Trong Nghia Nguyen<sup>1</sup>, Tuan Van Doan<sup>2</sup>,  
Thao Duong Vi<sup>2</sup>, Cong Long Nguyen<sup>3</sup>, Minh Viet Nguyen<sup>4</sup>, Chang-Ha Lee<sup>5,\*\*</sup>

<sup>1</sup>School of Chemical Engineering, Hanoi University of Science and Technology, Hanoi, Vietnam.

<sup>2</sup>R&D research center, Kangaroo Headquarter, Vietnam.

<sup>3</sup>Hepato-Gastroenterology Department, Bach Mai Hospital, Hanoi, Vietnam.

<sup>4</sup>Hanoi University of Industry, Vietnam.

<sup>5</sup>Department of Biomolecular and Chemical Engineering, Yonsei University, South Korea.

Received: 25<sup>th</sup> September 2019; Revised: 2<sup>nd</sup> February 2020; Accepted: 4<sup>th</sup> February 2020;

Available online: 28<sup>th</sup> February 2020; Published regularly: April 2020

## Abstract

This study aimed to synthesize Ag•ZnO•Activated carbon (Ag•ZnO•AC) composite from rice husk for degradation of dyes. The deposition of Ag and ZnO on AC led to decreasing the surface area and pore volume of Ag•ZnO•AC composite. In addition, when Ag and ZnO were dispersed on activated carbon, the Ag•ZnO flakes became denser and tighter, but the particle size of Ag became smaller from 5 to 7 nm. The photocatalytic ability of Ag•ZnO•AC composite was evaluated by degradation of Janus Green B (JGB) and compared with that of AC, ZnO, Ag•ZnO, and ZnO•AC samples. The effects of catalyst dosages, pH values, and initial dye concentrations on photocatalytic degradation were investigated in detail. The Ag•ZnO•AC composite had a high degradation efficiency of 100% in 60 min, showing the reaction rate of 0.120 min<sup>-1</sup> and degradation capacity of 17.8 mg/g within 20 min. The photocatalytic performance of the Ag•ZnO•AC composite was also evaluated by cyclic test and the degradation of other persistent dyes such as Methylene Blue, Tartrazine, Congo Red, and organic compounds (Caffeine and Bisphenol A). Based on the experimental results, the possible destruction route of JGB by the as-synthesized Ag•ZnO•AC composite was suggested. Copyright © 2020 BCREC Group. All rights reserved

**Keywords:** Rice husk; Silver; Zinc oxide; Activated carbon; Photocatalyst

**How to Cite:** Vu, A.-T., Pham, T.A.T., Tran, T.T., Nguyen, X.T., Tran, T.Q., Tran, Q.T., Nguyen, T.N., Doan, T.V., Vi, T.D., Nguyen, C.L., Nguyen, M.V., Lee, C.-H. (2020). Synthesis of Nano-Flakes Ag•ZnO•Activated Carbon Composite from Rice Husk as A Photocatalyst under Solar Light. *Bulletin of Chemical Reaction Engineering & Catalysis*, 15(1), 264-279 (doi:10.9767/bcrec.15.1.5892.264-279)

**Permalink/DOI:** <https://doi.org/10.9767/bcrec.15.1.5892.264-279>

## 1. Introduction

In developing countries, large amounts of wastewater are being discharged from various industries, such as: productions of coffee, beer, sugar, medicine, paper, rubber, cement, paint and textile [1]. Wastewater from each industry has its own characteristics, but it contains

heavy metals and persistent organic compounds. Since they are toxic to humans and pollute ecological seriously [2-4], wastewater must be treated before being discharged into the environment.

Zinc oxide (ZnO) has been known to oxidize harmful organic substances in wastewater effectively under the UV light irradiation. It was reported that photocatalytic ability of ZnO strongly depended on the morphology, which highly depended on the synthesis method. Nano-size

Corresponding Author.

\* E-mail: [tuan.vuanh@hust.edu.vn](mailto:tuan.vuanh@hust.edu.vn) (A.-T. Vu);

\*\* E-mail: [leech@yonsei.ac.kr](mailto:leech@yonsei.ac.kr) (C.-H. Lee)

ZnO synthesized by facile and fast method showed the highly effective degradation of tartrazine under UV light [5]. The hierarchical flower-like ZnO could degrade caffeine under UV light irradiation, showing up to 97.6% degradation within 120 min for caffeine solution of 5 mg/L [6]. When the nanowires ZnO, synthesized by the co-precipitation at the low temperature, was applied to acid red 57, the degradation efficiency was 90.03% within 200 min at the concentration of 30 mg/L [7].

It has been reported that the formation of heterojunction between Ag and ZnO particles could promote the separation and transfer efficiency of electron-hole on the surface of ZnO, leading to accelerate the generation rate of oxidized species ( $\text{OH}\cdot$  and  $\text{O}_2\cdot$ ) and degradation rate of organic pollutants. Therefore, many studies on doping Ag into ZnO have been reported [8-11]. Moreover, when carbon based materials like graphene oxide (GO), multi wall carbon nanotube (MWCNT), and AC were added into Ag-ZnO to improve the dispersion of Ag and ZnO particles, the photodegradation efficiency and stability of composites increased [12-18]. However, as seen in these reports, the researches only focused on synthesis of nanoparticles Ag and ZnO on carbon based materials. In addition, since the performance of catalyst was strongly depended on the morphology and the nano-flakes have a large junction surface, the nano-flakes Ag-ZnO on activated carbon is expected as an advanced catalyst for photodegradation of pollutant organic compounds.

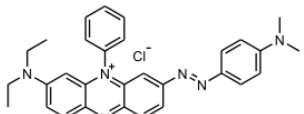
To treat waste water, high efficient photocatalysts are needed. Furthermore, since a large amount of waste water is emitted from industries, the cost of photocatalysts is also important as much as the efficiency of photodegradation. In addition, an enormous amount of rice husk (RH), a waste in the rice production,

is generated in agricultural countries. It was reported that world rice production is 489.1 million tons every year, which means approximately 122-163 million tons of rice husk biomass will be generated globally [19].

In Vietnam, since the rice is one of main agricultural crops, approximately 9 million tons of rice husk is generated into environment every year. Furthermore, since most of rice husk is burned or pored directly into the river and canal systems, it causes environmental damages as secondary pollutant [20]. The bulk density of RH is approximately  $100\text{--}122\text{ kg/m}^3$ , containing about 15-28 wt% of silica and 72-85 wt% of lignocellulose [21,22]. Therefore, to utilize RH properly, the studies to convert RH into silica or activated carbon have been widely performed [1,23-25]. Then, the developed porous material has been attracted for the great attention of water purification technology.

The objective of this study is synthesis of nano-flakes Ag-ZnO-AC composite from rice husk for degradation of dyes under solar light. As-synthesized samples were characterized by XRD, FE-SEM, HR-TEM, EDS, SEAD, FT-IR, and UV-vis diffuse reflectance, and  $\text{N}_2$  adsorption/desorption isotherms. The photocatalytic performance of as-prepared samples was evaluated for degrading Janus Green B, Methylene Blue, Tartrazine, Congo Red, Caffeine and Bisphenol A. In order to provide new insights into nano-flakes Ag-ZnO fabricated activated carbon, the performance was compared with that of AC, ZnO, Ag-ZnO and ZnO-AC. In this study, activated carbon with high surface area and pore volume was prepared from RH. And the activated carbon was fabricated with nano-flakes Ag-ZnO. The photocatalytic performance of as-prepared composites was evaluated for degrading JGB solution. To provide new insights into nano-flakes Ag-ZnO fabricated activated carbon, the performance was compared with that of AC, ZnO, Ag-ZnO, and ZnO-AC.

**Table 1.** Characteristics of Janus Green B.

Chemical formula	$\text{C}_{30}\text{H}_{31}\text{N}_6\text{Cl}$
Chemical class	Azo
Molecular weight (g/mole)	511.06
Color	Blue
$\lambda_{\text{max}}$ (nm)	611
C.I. number	11050
Nature	Cationic dye
Molecular structure	

## 2. Materials and Methods

### 2.1 Chemicals

Rice husk was obtained from a farm in Thai Binh Province of Vietnam. The characteristics of Janus Green B (JGB: 99.0%), purchased from Sigma-Aldrich, were presented in Table 1. Polyvinyl alcohol (PVA) (99.5%), glucose (99.0%), zinc acetate ( $\text{Zn}(\text{CH}_3\text{COO})_2 \cdot 2\text{H}_2\text{O}$ ) (99%), silver nitrate ( $\text{AgNO}_3$ ) (99.8%), hexamethylene tetramine (HMTA) (99%), sodium hydroxide (99.5%), liquid ammonia (28%),  $\text{TiO}_2$  (99.0%) and ZnO (99.0%) were obtained from

Merck. All chemicals were used without any further purification and double distilled water was used in all the experiments.

## 2.2 Preparation of Activated Carbon from Rice Husk

The method for preparation of activated carbon from RH was referred from previous report [26]. RH was washed with distilled water to remove soil and dust and then dried at 100 °C for 24 h. The dried RH was carbonized at 400 °C for 2 h at a heating rate of 5 °C/min to produce charcoal. Subsequently, charcoal was crushed by pestle and mortar and impregnated with 4M NaOH. The mixture was dried at 100 °C for 24 h. The obtained powder was calcined in a furnace under N<sub>2</sub> flow by two steps: (1) a ramp from room temperature to 400 °C at 8 °C/min and a soak at 400 °C for 1 h; (2) a ramp from 400 °C to 800 °C at 10 °C/min and a soak at 800 °C for 2 h. After cooling, the sample was washed with distilled water until pH reached neutral, then dried at 100 °C for 24 h. Finally, the activated carbon was obtained, which was denoted as AC.

## 2.3 Preparation of ZnO•AC Composite

ZnO•AC composite was prepared by using the procedure presented in previous work [27]. Typically, 2.19 g of zinc acetate and 0.7 g of HMTA were dissolved in 100 mL of distilled water, the pH solution was adjusted to 8.0 by liquid ammonia. 0.081 g of AC was added and then the suspension was stirred vigorously for 5 min. The mixture was transferred into a Teflon-lined autoclave and heated to 150 °C for 24 h. The product was washed several times with distilled water, then dried at 80 °C for 24 h. After being calcined in N<sub>2</sub> flow at 400 °C for 2 h with a heating rate of 5 °C/min, the black powder was changed to the grey powder, which was as ZnO•AC.

## 2.4 Preparation of Ag•ZnO•AC Composite

The synthesis procedure of Ag•ZnO•AC composite was referred in previous report [28] without using NaOH but with addition of PVA. 0.3564 g of ZnO•AC, 1 g of glucose and 0.2 g PVA were added together into 40 mL of distilled water, the temperature increased to 60 °C. To prepare the Ag•ZnO•AC composite at the Ag/ZnO molar ratio of 0.05, the optimal ratio for photocatalytic activity of nano Ag•ZnO under visible light irradiation that presented in previous report [29], 0.034 g of AgNO<sub>3</sub> was added into the mixture under vigorous stirring for

1 h. Finally, the powder was filtered and dried at 60 °C for 24 h, which was denoted as Ag•ZnO•AC.

## 2.5 Catalyst Characterizations

The crystalline phase of sample was investigated by X-ray power Diffraction (XRD: Bruker D8 Ax XRD-diffractometer, Germany). XRD patterns were obtained with Cu-K $\alpha$  irradiation (40kV, 40 mA) at the 2 $\theta$  ranging from 10 to 70°. The morphology and size of samples were observed by a Transmission Electron Microscopy (TEM, JEM-JEOL 2100), a Selected Area Electron Diffraction (SEAD, JEM-JEOL 2100), and a Field Emission Scanning Electron Microscopy (FE-SEM, JEOL-7600F). The chemical composition of a composite was determined by an Energy Dispersive Spectrometry (EDS: JEOL-7600F). The textural properties were measured via N<sub>2</sub> adsorption/desorption isotherms using a Quantachrome instrument (Autosorb iQ, version 3.0 analyzer). The specific surface area, pore volume and pore diameter were obtained by using the Brunauer-Emmett-Teller (BET) method. UV-vis diffuse reflectance spectra of the as-synthesized samples were measured on a UV-vis-NIR spectrometer (Cary 500). The composition of sample was measured by atomic absorption spectroscopy (AAS, NOVAA 350).

## 2.6 Catalytic Activity Studies

The experimental degradation of dye was conducted in a batch reactor. Typically, the certain amount of catalyst was added to a beaker with 100 mL of JGB solution at desired pH condition under magnetic stirring. The photocatalytic oxidation reaction was carried out directly under solar light irradiation in summer at 11:00 am-14:00 pm. The average intensity of solar light measured by a Lutron LX-101A light meter was about 82.600 LUX. pH solution was adjusted by 0.1 M HCl and 0.1 M NaOH solutions. At a given time interval, an aliquot (2 mL) of dye was withdrawn from the suspension and immediately filtered through a Millipore filter (0.45  $\mu$ m PTFE membrane) to separate solid particles. The dye concentration was analyzed by a UV-vis spectrophotometer (Agilent 8453) at the maximum absorbance wavelength dye. The degradation efficiency and capacity of dye were calculated by the following equations:

$$\text{Degradation efficiency (\%)} = \frac{C_0 - C_t}{C_0} \times 100\% \quad (1)$$

$$\text{Degradation capacity (mg/g)} = \frac{(C_0 - C_t) \times V}{m} \quad (2)$$

The degradation rate of dye was determined by fitting the degradation profile with the following first-order kinetic model:

$$\ln\left(\frac{C_0}{C_t}\right) = k_{ap} \times t \quad (3)$$

where  $k_{ap}$  ( $s^{-1}$ ) is the rate constant,  $C_0$  is the initial concentration of dye and  $C_t$  is the concentration of dye in time,  $V$  is the volume of dye solution (L),  $m$  is the mass of the adsorbent (g), and  $t$  is reaction time (min).

### 3. Results and Discussion

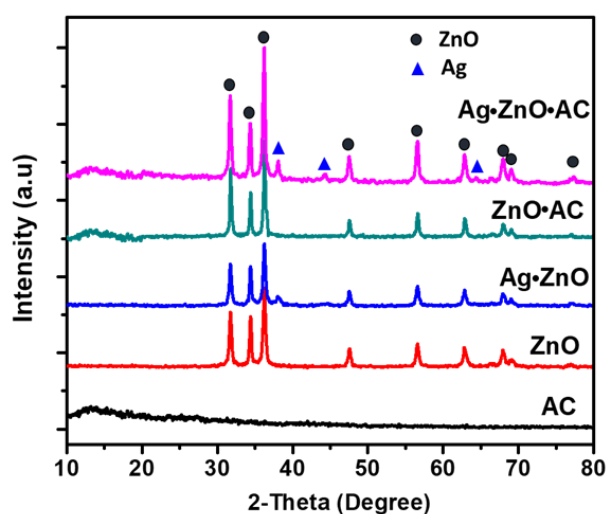
#### 3.1 Physicochemical Characterization

Figure 1 presents the SEM images, EDS mapping image, EDS spectrum, SEAD pattern, and HR-TEM images of as-synthesized samples. Activated carbon showed the lumps with a rough surface and approximately 10  $\mu\text{m}$  in size (Figure 1a). ZnO was observed in the shape of a thin sheet with the thickness of about 15 nm. The prepared zinc oxide was assembled from

many ZnO particles with many small holes of about 10 nm in size (Figure 1b). The Ag•ZnO sample became tighter and denser after loading the silver, in Figure 1c. In the ZnO•AC sample, ZnO particles with 20-30 nm in size were clearly observed, as shown in Figures 1d and e.

The Ag•ZnO flakes became thicker and denser when Ag•ZnO was deposited on AC (Figures 1f and g). Ag and ZnO were not clearly distinguished from the SEM images. On the other hand, the EDS mapping image (Figure 1h) showed a well dispersion of Ag and ZnO together on the surface of AC. The energy dispersive spectrometry (EDS) in Figure 1i showed the composition of 68.0 wt.% Zn, 15.8 wt.% O, 8.2 wt.% C and 8.2 wt.% Ag, which corresponded to molar ratio of Ag/ZnO of 0.09, showing larger than molar ratio from synthesis step (0.05). It could be assigned to either overlapping the peak of Ag with the peaks from other elements or analysis of surface of material by EDS method. However, the molar ratio of Ag/ZnO determined by atomic absorption spectroscopy (AAS) was 0.052. These results revealed that the well dispersion of Ag nano particles on surface of Ag•ZnO•AC composite. Ag nano particles with 20-30 nm in size, deposited on ZnO flakes, could be confirmed in TEM image in Ag•ZnO sample (Figure 1j). Both Ag and ZnO particles, well dispersed on AC and the dispersed Ag nanoparticles was smaller (about 5-7 nm) as seen in the TEM image for Ag•ZnO•AC composite (Figure 1k). The lattice planes (100), (101), (102), (110), (002), and (111) of hexagonal wurtzite structure ZnO was seen in Figure 1l. In addition, the crystal inter planar spacing was 0.23 nm (Figures 1m and n), which was attributed to the (111) planar spacing of Ag nanoparticle [30].

Figure 2 shows the wide-angle XRD diffraction of as-synthesized samples. The broad and low intensity of diffraction peak at  $13.4^\circ$  in the AC, ZnO•AC and Ag•ZnO•AC samples was assigned to activated carbon. The diffraction peaks at  $31.8$ ,  $34.2$ ,  $36.3$ ,  $47.5$ ,  $56.6$ ,  $62.6$ ,  $67.9$ ,



**Figure 2.** XRD patterns of the AC, ZnO, Ag•ZnO, ZnO•AC, and Ag•ZnO•AC samples.

**Table 2.** Textural properties of the AC, ZnO, Ag•ZnO, ZnO•AC and Ag•ZnO•AC samples.

Sample	$S_{\text{BET}}$ ( $\text{m}^2/\text{g}$ )	BJH meso pore volume ( $\text{cm}^3/\text{g}$ )	$t$ -plot micro- pore ( $\text{cm}^3/\text{g}$ )	Total pore volume ( $\text{cm}^3/\text{g}$ )	Average pore diameter (nm)	Crystallite size of Ag (nm)*	Crystallite size of ZnO (nm)*
AC	1620	1.060	0.011	1.071	7.6	-	-
ZnO	25.1	0.280	0.004	0.284	26.9	-	33.1
Ag•ZnO	24.2	0.207	0.003	0.210	21.8	15.1	36.2
ZnO•AC	142.1	0.410	0.007	0.417	4.2	-	25.1
Ag•ZnO•AC	128.2	0.328	0.005	0.333	3.8	8.2	13.3



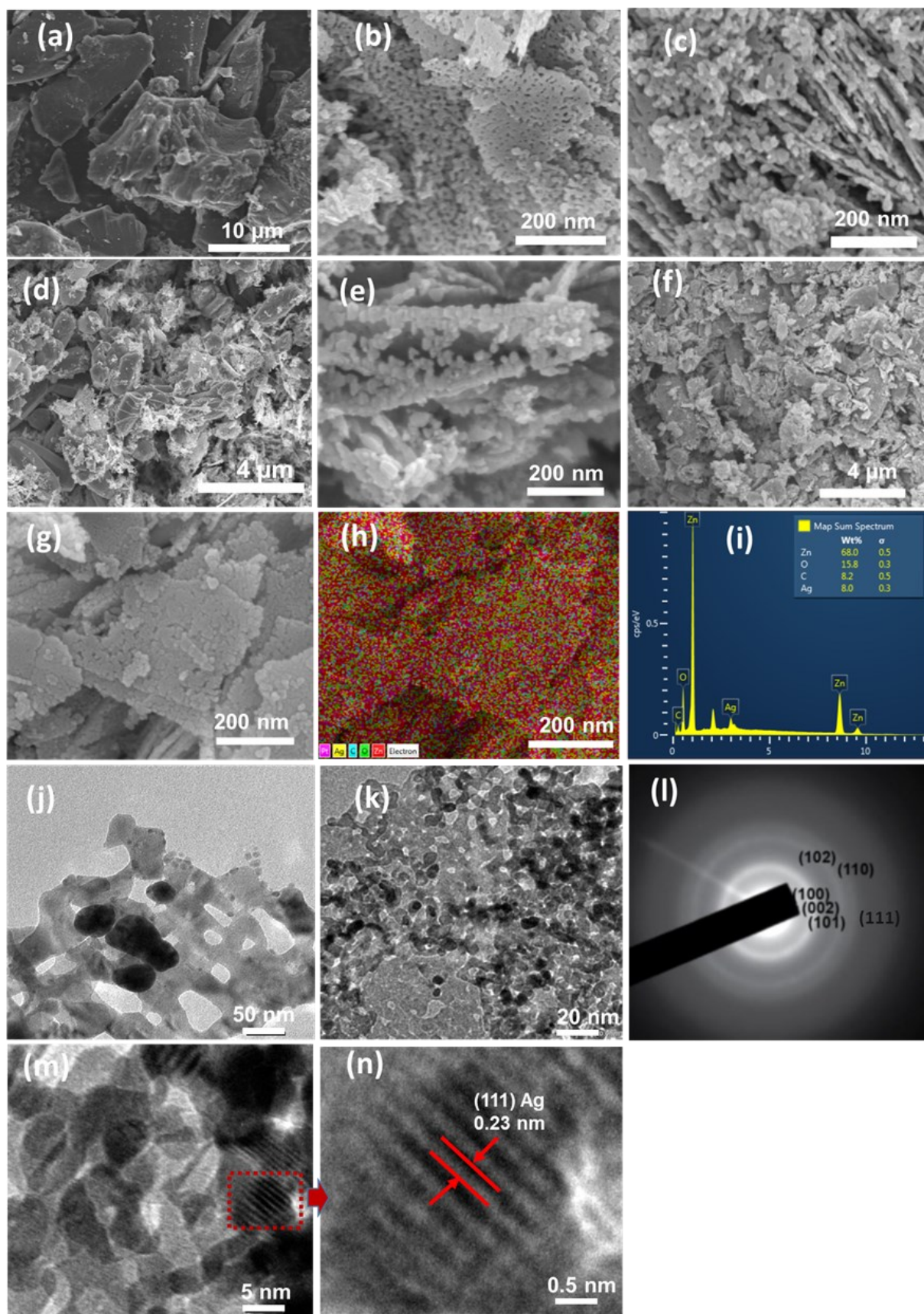


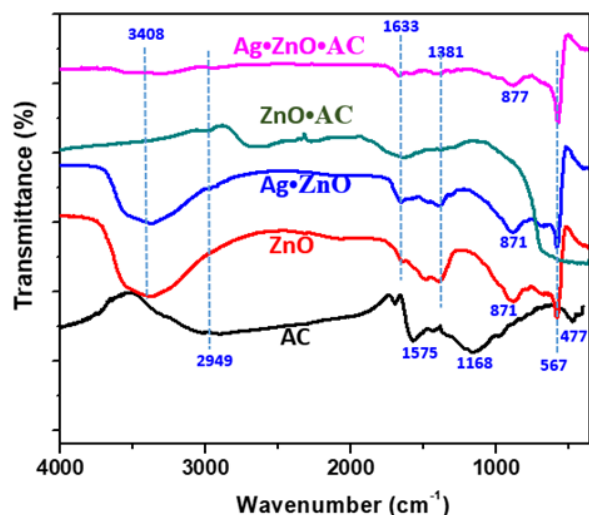
**Figure 1.** SEM images of (a) AC, (b) ZnO, (c) Ag·ZnO, (d) and (e) ZnO·AC, (f) and (g) Ag·ZnO·AC with different scale bars, (h) EDS mapping image and (i) EDS spectrum of Ag·ZnO·AC, (j) and (k) TEM images of Ag·ZnO and Ag·ZnO·AC, respectively, (l) SEAD pattern, and (m) and (n) HR-TEM images of Ag·ZnO·AC.

69.2 and 77.5° of ZnO, Ag·ZnO, ZnO·AC and Ag·ZnO·AC samples corresponded to (100), (002), (101), (102), (110), (103), (112), (201), and (202) plans, which were assigned to hexagonal wurtzite structure of ZnO (JCPDS no. 36-1451) [5]. The diffraction peaks at 38.2, 44.41, and 64.6°, in both Ag·ZnO and Ag·ZnO·AC samples, corresponding to (111), (220), and (311) plans, were attributed to face-centered cubic metallic Ag (JCPDS no. 04-0783) [10]. However, the intensity of peaks of Ag in the Ag·ZnO·AC composite was higher than that of the Ag·ZnO sample. The crystallite sizes of Ag and ZnO were calculated by Scherrer equation [31] in Table 2, which showed a consistent results with SEM and TEM analyses in Figure 1. The crystallite size of Ag in Ag·ZnO·AC com-

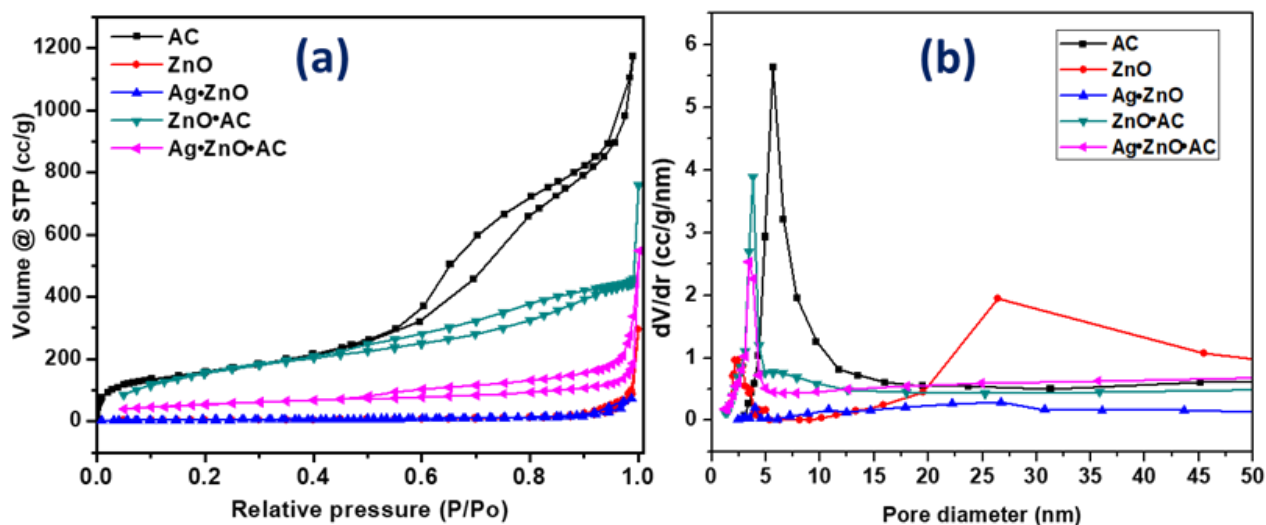
posite (8.2 nm) was smaller than that of Ag·ZnO (15.1 nm). In addition, no impurity peak was observed for all as-synthesized samples. The results confirmed the coexistence of ZnO and Ag in composite. When AC was added into composite, the crystallite size of Ag could be reduced but it did not influence to crystal structure of ZnO and Ag in Ag·ZnO·AC composite.

Figure 3 presents the FT-IR spectra of AC, ZnO, Ag·ZnO, ZnO·AC, and Ag·ZnO·AC samples. The bands at 1575 and 1168 cm<sup>-1</sup> of activated carbon could be assigned to C=O bond of carboxylic groups (-COOH) and the stretching vibration of conjugated C-C bonds of aromatic rings, respectively [32]. The broad band at 2949 cm<sup>-1</sup> in AC corresponded to the contribution from C-H bond vibration in aromatic compounds [33]. The strong band near 3408 cm<sup>-1</sup> in ZnO and Ag·ZnO samples could be assigned to O-H stretching vibration of absorbed water (H-O-H) [23]. Whereas, this band was not observed for AC, ZnO·AC, and Ag·ZnO·AC samples. The small band at 1633, 1381, and 877 cm<sup>-1</sup> of ZnO, Ag·ZnO, ZnO·AC, and Ag·ZnO·AC samples came from the vibration of O-H bond of Zn-O-H [6]. The intensity of these bands became lower in the order: AC>ZnO>Ag·ZnO>ZnO·AC>Ag·ZnO·AC. The intense band at 567 cm<sup>-1</sup> was ascribed to the Zn-O vibration of all ZnO, Ag·ZnO, ZnO·AC, and Ag·ZnO·AC samples [34].

Figure 4 presents the N<sub>2</sub> adsorption/desorption isotherms and pore size distributions of AC, ZnO, Ag·ZnO, ZnO·AC, and Ag·ZnO·AC samples. BET surface area, pore volume, and average pore size diameter of as-



**Figure 3.** FT-IR spectra of the AC, ZnO, Ag·ZnO, ZnO·AC, and Ag·ZnO·AC samples.



**Figure 4.** (a) N<sub>2</sub> adsorption/desorption isotherms, and (b) pore size distributions of the AC, ZnO, Ag·ZnO, ZnO·AC, and Ag·ZnO·AC samples.

synthesized samples are presented in Table 2. The isotherm of activated carbon was classified as a type IV based on the IUPAC system. In addition, activated carbon had a sharp H3 hysteresis loop containing a steep region associated with the closure of hysteresis loop at the relative pressure of  $\sim 0.5$ , in Figure 4a. It indicated a mesoporous material with slit-shape pores. The pore diameter of activated carbon was comparatively narrow concentrating at 5-10 nm (Figure 4b), showing the average pore size of 7.6 nm. The BET surface area, BJH meso pore volume, and  $t$ -plot micro pore volume were 1620 m<sup>2</sup>/g, 1.060, and 0.011 cm<sup>3</sup>/g, respectively (Table 2).

The hysteresis loop of ZnO and Ag•ZnO samples were extremely small in Figure 4a. Furthermore, the surface area and pore volume of ZnO and Ag•ZnO samples were much smaller than those of activated carbon. In addition, ZnO showed a bimodal pore size distribu-

tion, whereas Ag•ZnO sample had very wide pore size distribution due to tighter and denser composite as showed in Figure 1. However, the average pore diameters of ZnO and Ag•ZnO of 26.9 and 21.8 nm, respectively, were larger than that of activated carbon. The surface areas of ZnO•AC and Ag•ZnO•AC samples were 142.1 and 128.2 m<sup>2</sup>/g, respectively, even though the content of activated carbon in both samples was only 10 wt.%. Therefore, it was expected that activated carbon worked as a supporter for Ag and ZnO. They were well dispersed on the surface of activated carbon, as presented in HR-TEM and EDS images in Figure 1. Consequently, AC-based composite led to improve the surface area and pore volume with respect to ZnO and Ag•ZnO samples. On the other hand, the pore diameter of composite was significantly decreased due to the dispersion of small size Ag and ZnO particles on AC (Table 2).

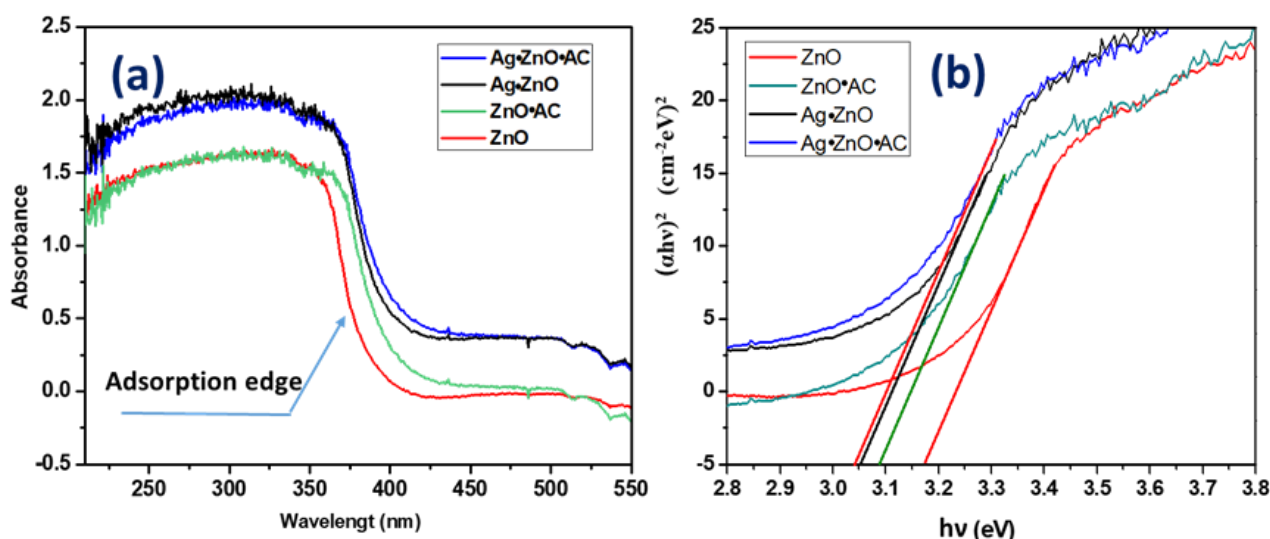


**Figure 5.** (a) UV-vis diffuse reflectance spectra and Tauc's plot of the ZnO, ZnO•AC, Ag•ZnO, and Ag•ZnO•AC samples.

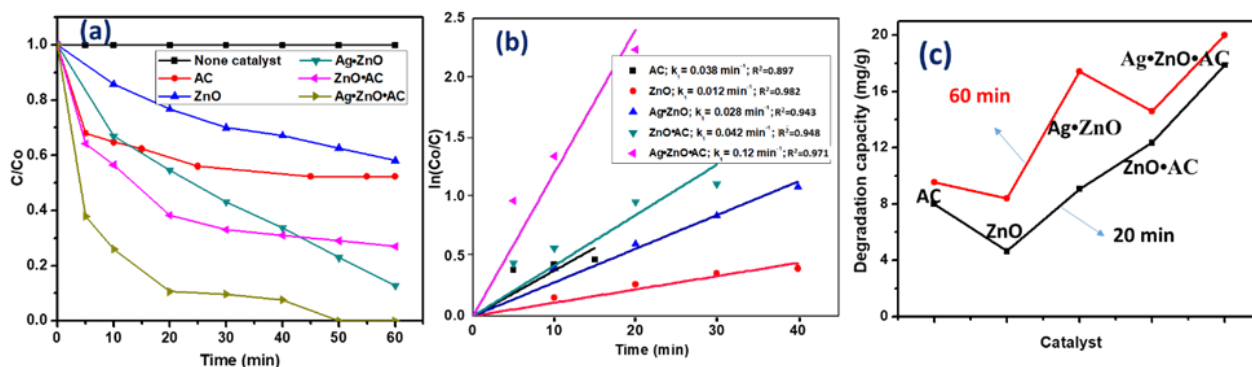


**Figure 6.** (a) Degradation of JGB at each catalyst under solar light, (b) fitting plots of first-order kinetic model in Equation (3), and (c) comparison of degradation capacity among catalysts. The reaction conditions: dosage catalyst of 0.5 g/L, JGB concentration of 10 mg/L, pH=6.5.



Figure 5 shows the UV-vis diffuse reflectance spectra and Tauc's plot of the ZnO, ZnO·AC, Ag·ZnO, and Ag·ZnO·AC samples. The presence of AC led to increase the absorption of ZnO·AC and Ag·ZnO·AC composites. The absorption edge shapes of the ZnO and ZnO·AC samples were similar, but when Ag was doped into ZnO and ZnO·AC the absorption of Ag·ZnO and Ag·ZnO·AC composites increased. The absorptions of as-prepared samples were in the order following:  $\text{ZnO} < \text{ZnO} \cdot \text{AC} < \text{Ag} \cdot \text{ZnO} < \text{Ag} \cdot \text{ZnO} \cdot \text{AC}$  (Figure 5a). The  $h\nu$  values were plotted against  $(ah\nu)^2$  and extended to calculate the band gap energy of the as-prepared samples by the Tauc's method [35], the results are presented in Figure 5b. The band gap energies of the ZnO, ZnO·AC, Ag·ZnO, and Ag·ZnO·AC were 3.16, 3.08, 3.04 and 3.01, respectively. The reduction in band gap energy of composite was assigned to both the dispersion of Ag and ZnO on AC and Ag doping into ZnO.

### 3.2 Degradation of Dyes

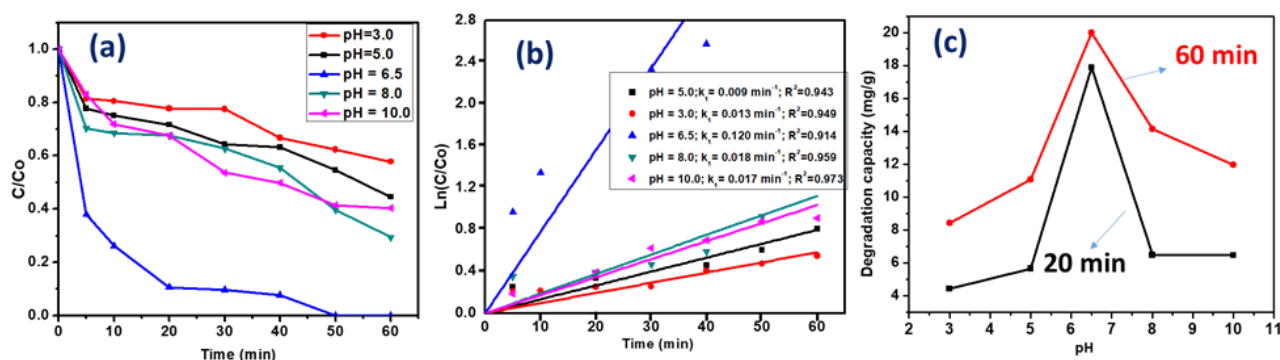
#### 3.2.1 Degradation of JGB in the different catalysts

Figure 6 shows the removal of JGB by various catalysts at the same reaction condition (dosage catalyst of 0.5 g/L, JGB concentration of 10 mg/L, and pH solution of 6.5). The degradation efficiency without any catalyst could be negligible. After activated carbon highly adsorbed JGB at initial 20 min (8.0 mg/g), the adsorption amount was smoothly increased with time. The adsorption capacity was saturated at 60 min, showing 9.5 mg/g in Figure 6c. The degradation of JGB by the ZnO and Ag·ZnO catalysts changed almost linearly with time, but the reaction rate and degradation capacity of JGB at 60 min by Ag·ZnO was higher than

those of ZnO, 0.012 min<sup>-1</sup> and 8.4 mg/g for ZnO, and 0.028 min<sup>-1</sup> and 17.4 mg/g for Ag·ZnO in Figure 6b. The degradation shape of JGB by ZnO·AC and Ag·ZnO·AC was similar with that of AC, the degradation capacities of ZnO·AC at 20 and 60 min were 12.4 and 14.6 mg/g, respectively, and the reaction rate was 0.042 min<sup>-1</sup>. However, the degradation efficiency and reaction rate of JGB by Ag·ZnO·AC composite were much higher than the others, showing the degradation efficiency of 100% at 60 min. In addition, the degradation capacity at 20 min was almost 90% (17.8 mg/g) and the reaction rate (0.120 min<sup>-1</sup>) was very fast, which was 50-100 times faster than ZnO and Ag·ZnO. The R<sup>2</sup> value from fitting degradation profile of JGB in Ag·ZnO·AC composite was lower than that of ZnO but lower than others. The low values of R<sup>2</sup> (0.879-0.982) could be assigned to the competition of processes of adsorption, penetration in pore, and photocatalytic reaction of on surface of JGB in as-synthesized catalysts. The results suggested that the addition of Ag into ZnO deposited activated carbon (Ag·ZnO·AC composite) could improve the photocatalytic activity of composite resulted from the reduction of band gap energy, as presented in Figure 5b.

#### 3.2.2 Effect of pH solution on degradation of JGB

The pH value of wastewater is an important factor for well designed reaction processes. It has a great influence not only on the functional groups and surface charges of adsorbents, but also the structure and ionization degree of pollutant molecules [36]. In this study, the effect of initial pH solution on degradation of JGB by the as-synthesized Ag·ZnO·AC sample was investigated. The performance was evaluated at a wide range of pH values from 3.0 to 10.0



**Figure 7.** (a) Effect of pH solution on degradation of JGB under solar light, (b) fitting plots of first-order kinetic model in Equation (3), and (c) degradation capacity at different pH values. The reaction conditions: dosage catalyst of 0.5 g/L, JGB concentration of 10 mg/L.

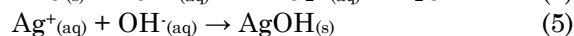
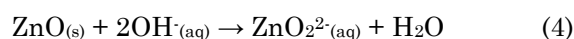


under the fixed other conditions (dosage catalyst of 0.5 g/L and JGB concentration of 10 mg/L).

Figure 7 presents the degradation of JGB with time at different pH values. The pH gave a critical impact on the degradation performance of JGB. When the pH value increased from 3.0 to 5.0, the degradation of JGB in composite slightly increased, showing the improved reaction rate from 0.009 to 0.013 min<sup>-1</sup> and the enhanced reaction capacity from 8.4 and 11.1 mg/g at 60 min (Figure 7b-c). At the pH value of 6.5, the degradation of JGB by the as-synthesized Ag•ZnO•AC composite significantly increased, degradation capacity at 60 min of 20 mg/g and reaction rate of 0.120 min<sup>-1</sup>. On the other hand, at higher than the pH value of 6.5, the reaction performance decreased significantly. At pH=8.0 and 10.0, the degradation capacities at 60 min were 14.1 and 11.9 mg/g and the reaction rates were 0.018 and 0.017 min<sup>-1</sup>, respectively, while the R<sup>2</sup> values were in range of 0.914-0.973.

It was reported that the pH of zero point charge for ZnO is approximately 9.0 (denoted as pH<sub>zpc</sub>) [37]. At lower pH than the pH<sub>zpc</sub> of ZnO, the stable suspension is formed because their net positive charge prevents agglomeration. Similar phenomena were observed when the pH values were higher than the pH<sub>zpc</sub> of ZnO, where the surface of ZnO particles could be negatively charged by absorbing OH<sup>-</sup> ions. In addition, the pH<sub>zpc</sub> of activated carbon was approximately 7.0 [38]. Therefore, the degradation rate of JGB was significantly enhanced with increasing the pH value from 3.0 to 6.5 in dye solution, because the electrostatic attraction between cationic JGB and negative charge surface of ZnO or AC could be enhanced. However, at the condition of higher than the pH value of 6.5, the significant decrease in the deg-

radation of JGB resulted from the dissolution of ZnO and precipitation of Ag<sup>+</sup> ion in alkaline medium by the following equations:



The results indicated the important contribution of activated carbon to the degradation of JGB. Since JGB molecules are adsorbed on activated carbon at the pH value of 6.5 more than the other pH values, more concentrated JGB molecules can contact with Ag•ZnO. Therefore, the degradation performance at the pH value of 8.0, which is the value between the pH<sub>zpc</sub> values of activated carbon and ZnO. Such contribution of activated carbon to the degradation of JGB could be also observed in Figure 6, showing higher degradation of JGB in ZnO•AC than in Ag•ZnO.

### 3.2.3 Effect of catalyst dosage on degradation of JGB

To investigate the influence of catalyst amount on the degradation performance, the experiments were carried out by employing different catalyst dosage (0.25, 0.5, 0.75, and 1.0 g/L) under constant reaction conditions: JGB concentration of 10 mg/L and pH=6.5. The degradation efficiency of JGB increased with an increase in dosage catalyst as shown in Figure 8. The degradation efficiencies of JGB in the Ag•ZnO•AC composite at 0.25 g/L were 52.1 and 69.8%, in 20 and 60 min, respectively. The degradation efficiency in 20 min increased to 89.3, 93.2 and 99.7% at dosage catalysts of 0.5, 0.75 and 1.0 g/L, respectively. Furthermore, the degradation performance was approached 100% before 60 min except the case of 0.25 g/L in Figure 8a. In addition, the appreciable in-

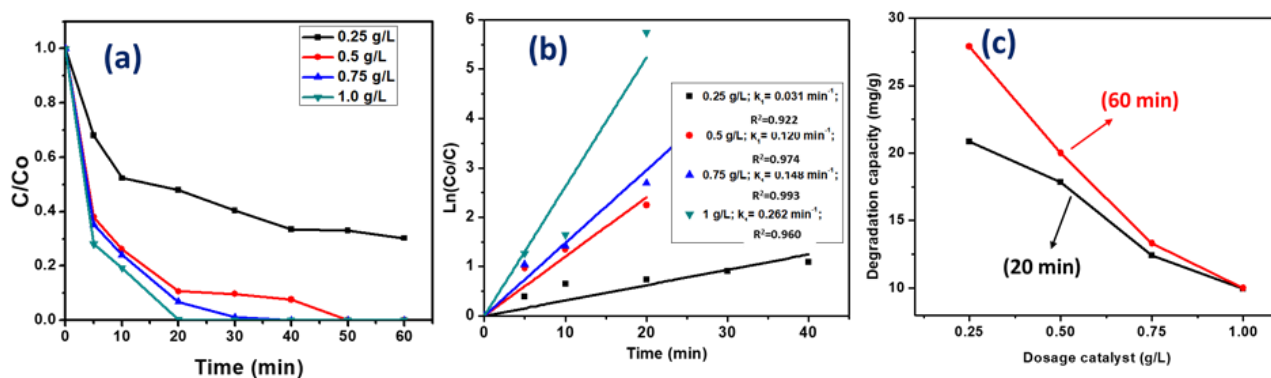


**Figure 8.** (a) Effect of catalyst dosage on degradation of JGB, (b) fitting plots of first-order kinetic model in Equation (3), and (c) degradation capacity versus dosage catalyst. The reaction conditions: JGB concentration of 10 mg/L, and pH=6.5.

crease in reaction rate of JGB was observed with increasing the catalyst dosage, the  $R^2$  values were in range of 0.922-0.993 (Figure 8b).

Since the increase of catalyst dosage leads to an increase in the number of active sites on surface of catalysts, the density of catalyst particles in the area of illumination is improved [39]. However, the degradation capacity of JGB per gram of catalyst was decreased with an increase in catalyst dosage, as shown in Figure 8(c), due to increasing the suspended catalysts in a solution. The short wave tail photons are not able to enter the reaction mixture and a decrease in sunlight light penetration resulting an increase in scattering effect [40,41]. In addition, as more catalyst was added, each catalyst has less chance to contact with JGB molecules because of fast reaction as shown in Figure 8a. As a result, the reaction performance and rate can be improved with increasing catalyst dosage, but degradation capacity became smaller.

### 3.2.4 Effect of dye concentration on degradation of JGB

The impact of various dye concentration on the photocatalytic degradation was studied by varying the concentration of JGB from 5 to 20 mg/L. The dosage of the Ag·ZnO·AC composite and pH value were fixed at 0.5 g/L and 6.5, respectively. In Figure 9, the degradation efficiency and reaction rate were decreased significantly with an increase in initial dye concentration. At the concentration of 5 mg/L, the degradation efficiency at 20 min and reaction rate were 99.8% and  $0.515 \text{ min}^{-1}$ , respectively. Whereas, the degradation efficiency and reaction rate at 20 mg/L were only 43.1% and  $0.030 \text{ min}^{-1}$ . The  $R^2$  values were in range of 0.920-0.973 in Figure 9b.

The negative effect of increased mount JGB on reaction can be interpreted by the following reasons: (1) The number of JGB molecules, adsorbed on the active sites of the catalyst surface, increase with the initial concentration of

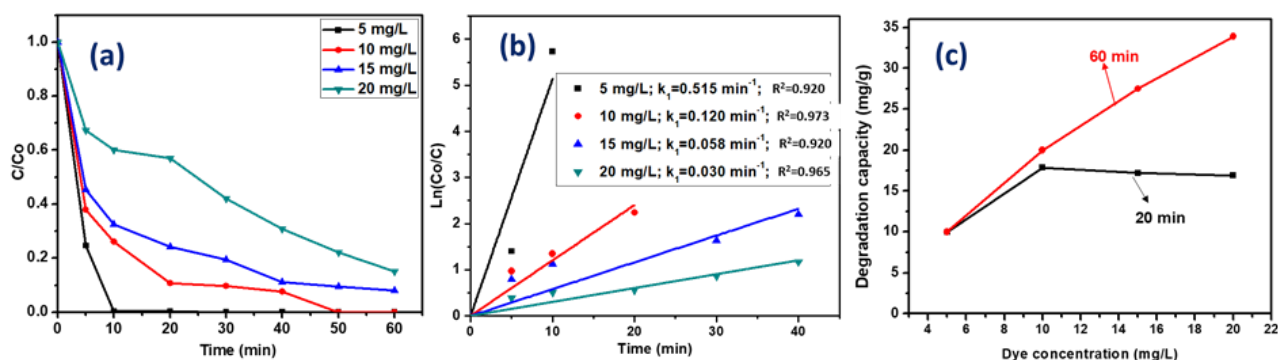


**Figure 9.** (a) Effect of initial dye concentration on degradation of JGB, (b) fitting plots of first-order kinetic model in Equation (3), and (c) degradation capacity. The reaction conditions: Dosage catalyst of 0.5 g/L; pH= 6.5.

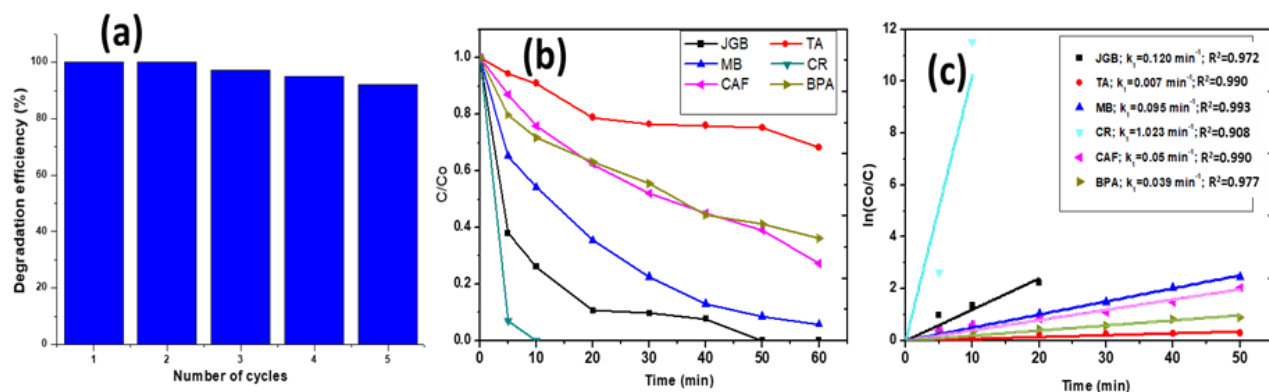


**Figure 10.** (a) Removal efficiency of Ag·ZnO·AC composite in five successive cycles, (b) the degradation of other organic dyes on as-synthesized Ag·ZnO·AC composite and (c) fitting plots of first-order kinetic model in Equation (3). The reaction conditions: dosage catalyst of 0.5 g/L; dye concentration of 10 mg/L; pH =6.5.

JGB dye. Therefore, the generation rate of  $O_2^{\bullet}$ , and  $OH^{\bullet}$  radicals on the same active sites became decreased; (2) Alternatively, increasing the dye concentration lead to generating a large number of intermediates form dye molecules along with the reaction, and may compete with JGB molecules in the constant total active sites; (3) Otherwise, with an increase in the initial dye concentration, the solution becomes more intensely colored and the path length of photons by the catalyst decreases, and consequently the degradation rate is reduced. Despite lowering in degradation efficiency and reaction rate of JGB with increasing the initial concentration of dye, the degradation capacity at 10 mg/L during 20 min (17.8 mg/g) was higher than that of other concentrations, but the degradation capacity at 60 min increased with the initial concentration of JGB (Figure 9c). Furthermore, it was expected that the degradation efficiency can be achieved to 100% regardless of initial concentrations if the reaction time is elongated as shown in Figure 9a.

### 3.2.5 Photocatalytic stability of catalyst

The photostability of a catalyst is one of important factors from industrial perspectives.

Five repeated experiments were performed on the fresh JGB solution in every run with the same dosage of the as-synthesized  $Ag^{\bullet}ZnO^{\bullet}AC$  composite under solar light irradiation. In each experimental run, the catalyst was reused after being centrifuged, washed with distilled water and dried at 60 °C. The stability of as-synthesized composite is displayed in Figure 10a. The photocatalytic activity of the  $Ag^{\bullet}ZnO^{\bullet}AC$  composite was slightly decreased, but it still remained at 92% for the fifth experiment.

### 3.2.6 The degradation of other dyes and organic compounds and comparison with other catalysts

The degradation efficiency of organic compounds by photocatalysts depends not only catalyst properties, such as: surface area, pore volume and pore size distribution, and composition, but also the characteristics of organic compounds. Therefore, the optimum condition for degradation of certain organic compound depends on the characteristics of catalyst and solution conditions.

In this study, the photocatalytic performance of the as-synthesized  $Ag^{\bullet}ZnO^{\bullet}AC$  com-

**Table 3.** Comparison of degradation of JGB by various materials.

Catalyst	Reaction conditions	Observation	Reference
$Fe_2O_3 \cdot SiO_2/H_2O_2$	[Cat.] = 0.5 g/L, [JGB] = 50 mg/L, $[H_2O_2]$ = 12 mM, pH = 3.0	71.2% of dye was removed in 80 min, degradation capacity in 80 min of 98.5 mg/g.	[23]
Hierarchical flower-like ZnO	[Cat.] = 3 g/L, [JGB] = 10 mg/L, pH = 7.0, under UV light irradiation	95.7% of dye was removed in 40 min	[6]
$Fe_2O_3/Cu_2O$ composite	[Cat.] = 0.75 g/L, [JGB] = 9 mM, pH = 5.0, under visible light irradiation	Approximately 95% of dye was removed in 120 min	[42]
$LaMnO_3$	[Cat.] = 1 g/L, [JGB] = 20 mg/L, pH = 2.7	Approximately 32 and 45% under dark and visible light, respectively	[43]
$LaFeMn_{0.5}O_3$	[Cat.] = 1 g/L, [JGB] = 20 mg/L, pH = 2.7	Approximately 15 and 15% under dark and visible light, respectively	[43]
Commercial ZnO	[Cat.] = 0.5 g/L, [JGB] = 10 mg/L, pH = 6.5, under solar light irradiation	38.1% of dye was removed in 60 min	This work
Commercial $TiO_2$	[Cat.] = 0.5 g/L, [JGB] = 10 mg/L, pH = 6.5, under solar light irradiation	32.2% of dye was removed in 60 min	This work
$Ag^{\bullet}ZnO^{\bullet}AC$ composite	[Cat.] = 0.5 g/L, [JGB] = 10 mg/L, pH = 6.5, under solar light irradiation	100% of dye was removed in 60 min, degradation capacity in 20 min of 17.8 mg/g.	This work

posite was evaluated by other dyes, such as: Congo red (CR), Methylene blue (MB), and Tartrazine (TA), and organic compounds, such as: Caffeine (CAF) and Bisphenol A (BPA), at the optimal conditions for JGB (dosage catalyst of 0.5 g/L, dyes concentration of 50 mg/L, pH solution of 6.5). As shown in Figures 10b and c, the reaction efficiency and rate were  $TA < BPA < CAF < MB < JGB < CR$  and the  $R^2$  values were larger than 0.908. The reaction rate and efficiency of TA dye at 60 min ( $0.007 \text{ min}^{-1}$  and 31.8%, respectively) were much lower than those of CR ( $1.023 \text{ min}^{-1}$  and 100%, respectively).

The catalytic performance for degradation of JGB in the as-synthesized  $Ag \cdot ZnO \cdot AC$  composite was compared with different catalysts from recent literatures [6,23,42,43]. The reaction condition and degradation efficiency of these catalysts are listed in Table 3. The degradation efficiency of the  $Ag \cdot ZnO \cdot AC$  composite was higher than those of commercial  $TiO_2$  and  $ZnO$  with the same reaction conditions. The directed comparison of the  $Ag \cdot ZnO \cdot AC$  composite with other catalysts is challenging since each study evaluated the removal capacity under different conditions. But, the relative per-

**Table 4.** Comparison of degradation of organic compounds by Ag-ZnO/carbon based catalyst.

Catalyst	Morphology	BET surface area ( $\text{m}^2/\text{g}$ )	Reaction conditions	Observation	Reference
Ag-ZnO/CNS	Ag-ZnO nanoparticles on nanospheres (100-300 nm)	-	[Cat.] = 0.08 g/L, [Methylene blue] = 50 mg/L, under UV light, the intensity of light source of $713.37 \text{ mW}/\text{cm}^2$	Degradation efficiency in 15 min of 95%, it was slightly decreased after fifth cyclic test (approximately 90%)	[12]
Ag-ZnO/MWCNT	Ag-ZnO nanoparticles (<100 nm) on MWCNT	23	[Cat.] = 1 g/L, [Acid orange 7] = 20 mg/L, pH = 5.0, under visible light (Halogen-Tungsten lamp 400 W)	Degradation efficiency in 120 min of 98%, it was slightly decreased after 4 <sup>th</sup> cyclic test (95%)	[13]
Ag-ZnO/GO	Ag-ZnO nanoparticles on surface of GO	-	[Cat.] = 1 g/L, [Methylene blue] = 15 mg/L, pH = 8.5-9.0	Degradation efficiencies in 180 min of 58 and 99% under visible light and UV light, respectively, it was remarkably decreased after 8 <sup>th</sup> cyclic test (52%)	[14]
Ag-ZnO/GO	Ag and ZnO nanoparticles on surface of GO	-	[Cat.] = 0.25 g/L, [Naphthalene] = 50 mg/L, under visible light (Xe lamp 250 W)	Degradation efficiency in 30 min of 92%, it was relatively decreased after 5 <sup>th</sup> cyclic test (85%)	[15]
Ag-N-ZnO/CHAC	ZnO nanoparticles co-dope with Ag and N on coconut husk AC	472	[Cat.] = 0.2 g/L, [methyl orange] = 30 mg/L, under visible light (Xe lamp 500 W)	Degradation efficiency in 120 min of 98.8%, it was slightly decreased after fifth cyclic test (approximately 94.3%)	[16]
Ag-ZnO/AC	Ag-ZnO nanoparticles on commercial AC	-	[Cat.] = 0.4 g/L, [Methyl orange] = 10 mg/L, pH = .0, UV light (Hg lamp 500 W)	Degradation efficiency in 150 min of 96%	[17]
Ag-ZnO/AC	Ag nanoparticles on surface of ZnO/AC	29.1	[Cat.] = 2 g/L, [Bisphenol-A] = 5 mg/L, $[H_2O_2]$ = 20 ml/L, under visible light (Xe Lamp 51 W)	Degradation efficiency in 100 min approximately 99%, it was remarkably decreased after 5 <sup>th</sup> cyclic test (85%)	[18]
$Ag \cdot ZnO \cdot AC$ composite	Ag-ZnO nano-flakes on AC	128	[Cat.] = 0.5 g/L, [JGB] = 10 mg/L, pH = 6.5, under solar light	Degradation efficiency in 60 min of 100%, it was slightly decreased after 5 <sup>th</sup> cyclic test (92%), the catalyst capacity in 20 min of 17.8 mg/g	This work



formance of the Ag•ZnO•AC composite can be evaluated indirectly. The degradation efficiency of JGB on Ag•ZnO•AC composite was higher than those of other catalysts. The degradation efficiency of the Ag•ZnO•AC composite in 20 min was lower than that of Fe<sub>2</sub>O<sub>3</sub>•SiO<sub>2</sub>/H<sub>2</sub>O<sub>2</sub>, but it takes basic solution to neutralize the wastewater (pH=3.0) after treatment and spends H<sub>2</sub>O<sub>2</sub> solution to generate OH• with Fenton-like catalyst Fe<sub>2</sub>O<sub>3</sub>•SiO<sub>2</sub>/H<sub>2</sub>O<sub>2</sub>. Therefore, the Ag•ZnO•AC composite prepared from rice husk is expected as a cheap and eco-friendly catalyst for large scale application.

The comparative results of degradation of pollutant organic compounds by Ag-ZnO on carbon based materials are presented in Table 4. The degradation efficiency and stability of catalysts depended on morphology, carbon based material, reaction condition. The Ag-ZnO on carbon nanospheres (Ag-ZnO/CNS) showed a fast reaction rate, the degradation efficiency of 95% in 15 min, it was slightly decreased after fifth cyclic test (approximately 90%). The Ag-ZnO nanoparticles on graphene oxide (Ag-ZnO/GO) showed a high degradation efficiency, but the stability was lower than those of Ag-ZnO nanoparticles on MWCNT (Ag-ZnO/MWCNT) and Ag-ZnO nanoparticles on AC (Ag-ZnO/AC). Although the surface area of the nano-flakes Ag-ZnO on AC (Ag•ZnO•AC) was significantly lower than that of ZnO nanoparticles co-dope with Ag and N on coconut husk AC (Ag-N-ZnO/CHAC), the degradation efficiency and stability were similar to each other.

### 3.3 Reaction Mechanism

The UV-vis spectral change of JGB and the colour of dye solution were measured at the time interval of 10 min during degradation in Figure 11a. Before oxidation ( $t = 0$ ), the absorption spectra of JGB was characterized by the bands in the ultraviolet region at 288 and 393 nm and by another band in visible region at 611 nm. The peak at 288 nm is due to benzene-like structure in the molecules while the bands in the visible region were associated with the chromophore containing azo linkage [27]. The disappearance of the absorbance peak at 611 nm with the reaction time could stem from the fragmentation of the azo links by oxidation [44]. The decrease in intensity of band at 393 nm could be attributed to breaking the -N-C-bond [23]. In addition to this rapid degradation, the decay of the absorbance at 288 nm was considered as the evidence of degradation of aromatic fragments in the dye molecule and its intermediates. Moreover, the different base line in UV-vis spectra was observed, but the maximum absorption had no displacement, it was assigned to formation of intermediate products. According to the UV-vis absorption spectra, the possible route of the destruction of JGB by as-synthesized Ag•ZnO•AC composite was suggested in Figure 11b.

### 4. Conclusion

AC with the high surface area (1620 m<sup>2</sup>/g) and pore volume (1.071 cm<sup>3</sup>/g) was prepared from RH, then it was fabricated with nano-

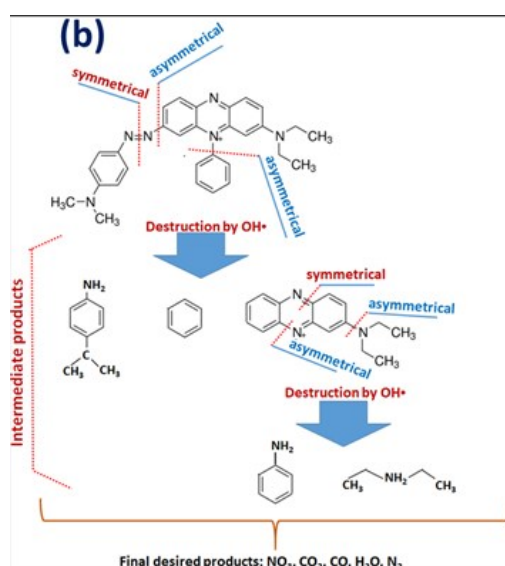
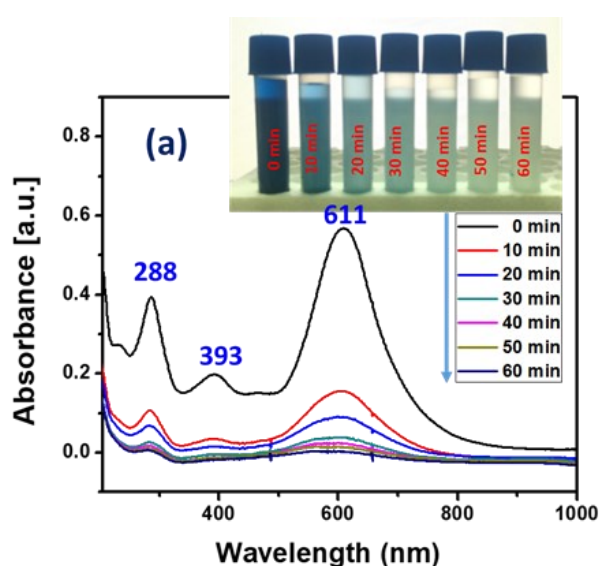


**Figure 11.** (a) UV-vis spectral change of JGB during degradation along reaction time and (b) possible route to the destruction of JGB by as-synthesized Ag•ZnO•AC catalyst. Reaction conditions: dosage catalyst of 0.05 g/L, dye concentration of 10 mg/L, and pH = 6.5.

flakes Ag•ZnO (Ag•ZnO•AC) as a photocatalyst. The physical properties and performance of Ag•ZnO•AC was compared to those of ZnO, Ag•ZnO, and ZnO•AC. The as-prepared ZnO sample with 15 nm in thickness contained and many holes with the diameter of 10 nm. Ag nano particles with 20-30 nm in size were deposited on ZnO flakes. And, both Ag and ZnO particles, well dispersed on AC and the dispersed Ag nanoparticles was smaller (about 5-7 nm), leading to a decrease in band gap energy but the photocatalytic activity of composite increased.

The degradation efficiency in 60 min, reaction rate, and degradation capacity in 20 min of the Ag•ZnO•AC of 100%, 0.120 min<sup>-1</sup>, and 17.8 mg/g, respectively, were higher than those of other samples (ZnO, ZnO•AC, and Ag•ZnO). The catalytic activity of Ag•ZnO•AC composite at pH solution of 6.5 were higher than those of other pH values. The degradation efficiencies of JGB in the Ag•ZnO•AC composite at 0.25 g/L were 52.1 and 69.8%, in 20 and 60 min, respectively. When dosage catalyst increased the degradation efficiency and reaction rate increased due to increasing the number of active sites of surface of catalyst. The degradation efficiency in 20 min increased to 89.3, 93.2 and 99.7% at dosage catalysts of 0.5, 0.75 and 1.0 g/L, respectively. Whereas the degradation capacity in 20 and 60 min were decreased due to increasing the suspended catalysts in a solution. The degradation efficiency and reaction rate were decreased, but the degradation capacity in 60 min increased when the JGB concentration increased from 5 to 20 mg/L. The degradation capacity in 20 min at 10 mg/L were higher than that at other concentrations.

The Ag•ZnO•AC composite showed a high stability in cyclic experiment, the degradation efficiency was still remained at 92% for the fifth cyclic experiment. The Ag•ZnO•AC composite also exhibited a high effectivity of photocatalyst for other dyes (MB, CR, and TA) and persistent organic compounds (CAF and BPA). In addition, the degradation route of JGB in Ag•ZnO•AC composite was proposed.

### Acknowledgments

The authors are grateful for the financial support from Vietnamese Ministry of Education and Training under grant number B2017-BKA-53, and Vietnam National Foundation for Science and Technology Development (NAFOSTED) under grant number 104.05-2018.333.

### References

- [1] Thu, H.T., Dat, L.T., Tuan, V.A. (2019). Synthesis of mesoporous SiO<sub>2</sub> from rice husk for removal of organic dyes in aqueous solution. *Vietnam Journal of Chemistry*, 57,175-181.
- [2] Ahmed, M.A., El-Katori, E.E., Gharni, Z.H. (2013). Photocatalytic degradation of methylene blue dye using Fe<sub>2</sub>O<sub>3</sub>/TiO<sub>2</sub> nanoparticles prepared by sol-gel method. *J. Alloys Compd.*, 553, 19-29.
- [3] Akpan, U.G., Hameed, B.H. (2009). Parameters affecting the photocatalytic degradation of dyes using TiO<sub>2</sub>-based photocatalysts: A review. *J. Hazard. Mater.*, 170, 520-529.
- [4] Le, M.T., Nguyen, H.L., Vu, A.-T., Nguyen, V.C., Wu, J.C.S. (2019). Synthesis of TiO<sub>2</sub> on different substrates by chemical vapor deposition for photocatalytic reduction of Cr(VI) in water. *Journal of the Chinese Chemical Society*, 66, 1713-1720.
- [5] Tu, V.A., Tuan, V.A. (2018). A facile and fast solution chemistry synthesis of porous ZnO nanoparticles for high efficiency photodegradation of tartrazine. *Vietnam Journal of Chemistry*, 56, 214-219.
- [6] Mai, L.T., Hoai, L.T., Tuan, V.A. (2018). Effects of reaction parameters on photodegradation of caffeine over hierarchical flower-like ZnO nanostructure. *Vietnam Journal of Chemistry*, 56, 647-653.
- [7] Kiwaan, H.A., Atwee, T.M., Azab, E.A., El-Bindary, A.A. (2019). Efficient photocatalytic degradation of Acid Red 57 using synthesized ZnO nanowires. *Journal of the Chinese Chemical Society*, 66, 89-98.
- [8] P. Fageria, S. Gangopadhyay, S. Pande, Synthesis of ZnO/Au and ZnO/Ag nanoparticles and their photocatalytic application using UV and visible light, *RSC Advances* 4 (2014) 24962-24972.
- [9] Sarma, B., Sarma, B.K. (2017). Fabrication of Ag/ZnO heterostructure and the role of surface coverage of ZnO microrods by Ag nanoparticles on the photophysical and photocatalytic properties of the metal-semiconductor system. *Applied Surface Science*, 410, 557-565.
- [10] Wang, L., Hou, X., Li, F., He, G., Li, L. (2015). Hybrid ZnO/Ag nanocomposites: Fabrication, characterization, and their visible-light photocatalytic activity. *Mater. Lett.*, 161, 368-371.
- [11] Zhai, H., Wang, L., Sun, D., Han, D., Qi, B., Li, X., Chang, L., Yang, J. (2015). Direct sunlight responsive Ag-ZnO heterostructure photocatalyst: Enhanced degradation of rhodamine B. *Journal of Physics and Chemistry of Solids*, 78, 35-40.

- [12] Singhal, S., Dixit, S., Shukla, A.K. (2018). Self-assembly of the Ag deposited ZnO/carbon nanospheres: A resourceful photocatalyst for efficient photocatalytic degradation of methylene blue dye in water. *Advanced Powder Technology*, 29, 3483-3492.
- [13] Moradi, M., Haghighi, M., Allahyari, S. (2017). Precipitation dispersion of Ag-ZnO nanocatalyst over functionalized multiwall carbon nanotube used in degradation of Acid Orange from wastewater. *Process Safety and Environmental Protection*, 107, 414-427.
- [14] Thi, V.H.T., Cao, T.H., Pham, T.N., Pham, T.T., Le, M.C. (2019). Synergistic Adsorption and Photocatalytic Activity under Visible Irradiation Using Ag-ZnO/GO Nanoparticles Derived at Low Temperature. *Journal of Chemistry*, 2019, 1-13.
- [15] Mukwevho, N., Gusain, R., Fosso-Kankeu, E., Kumar, N., Waanders, F., Ray, S.S. (2020). Removal of naphthalene from simulated wastewater through adsorption-photodegradation by ZnO/Ag/GO nanocomposite. *Journal of Industrial and Engineering Chemistry*, 81, 393-404.
- [16] Chen, X., Wu, Z., Gao, Z., Ye, B.-C. (2017). Effect of Different Activated Carbon as Carrier on the Photocatalytic Activity of Ag-N-ZnO Photocatalyst for Methyl Orange Degradation under Visible Light Irradiation. *Nanomaterials*, 7, 258-275.
- [17] Yin, D., Le, Z., Liu, B., Wu, M. (2012). Ag/ZnO-C nanocomposite-preparation and photocatalytic properties. *Journal of nanoscience and nanotechnology*, 12, 2248-2253.
- [18] Intarasuwan, K., Amornpitoksuk, P., Suwanboon, S., Graidist, P., Maungchanburi, S., Randorn, C. (2018). Effect of Ag loading on activated carbon doped ZnO for bisphenol A degradation under visible light. *Adv. Powder Technol.*, 29, 2608-2615.
- [19] Chen, H., Wang, W., Martin, J.C., Oliphant, A.J., Doerr, P.A., Xu, J.F., DeBorn, K.M., Chen, C., Sun, L. (2013). Extraction of Lignocellulose and Synthesis of Porous Silica Nanoparticles from Rice Husks: A Comprehensive Utilization of Rice Husk Biomass. *ACS Sustainable Chemistry & Engineering*, 1, 254-259.
- [20] Korobochkin, V.V., Tu, N.V., Hieu, N.M. (2016). Production of activated carbon from rice husk Vietnam. *IOP Conference Series: Earth and Environmental Science*, 43, 012066.
- [21] Quispe, I., Navia, R., Kahhat, R. (2017). Energy potential from rice husk through direct combustion and fast pyrolysis: A review. *Waste Manage. (Oxford)*, 59, 200-210.
- [22] Shen, Y. (2017). Rice husk silica derived nanomaterials for sustainable applications. *Renewable and Sustainable Energy Reviews*, 80, 453-466.
- [23] Vu, A.-T., Xuan, T.N., Lee, C.-H. (2019). Preparation of mesoporous Fe<sub>2</sub>O<sub>3</sub>/SiO<sub>2</sub> composite from rice husk as an efficient heterogeneous Fenton-like catalyst for degradation of organic dyes. *Journal of Water Process Engineering*, 28, 169-180.
- [24] Sugashini, S., Begum, K.M.M.S. (2015). Preparation of activated carbon from carbonized rice husk by ozone activation for Cr (VI) removal. *Carbon*, 93, 1086-1087.
- [25] Menya, E., Olupot, P.W., Storz, H., Lubwama, M., Kiros, Y. (2018). Production and performance of activated carbon from rice husks for removal of natural organic matter from water: A review. *Chemical Engineering Research and Design*, 129, 271-296.
- [26] Le Van, K., Luong Thi, T.T. (2014). Activated carbon derived from rice husk by NaOH activation and its application in supercapacitor. *Progress in Natural Science: Materials International*, 24, 191-198.
- [27] Van, N.T., Tuan, V.A. (2018). Photodegradation of Janus Green B on zinc oxide nano particles loaded on activated carbon preparation from rice husk. *Vietnam Journal of Chemistry*, 56, 306-311.
- [28] Sun, F., Tan, F., Wang, W., Qiao, X., Qiu, X. (2012). Facile synthesis of Ag/ZnO heterostructure nanocrystals with enhanced photocatalytic performance. *Materials Research Bulletin*, 47, 3357-3361.
- [29] Wang, H., Liu, X., Han, S. (2016). The synthesis of a Ag-ZnO nanohybrid with plasmonic photocatalytic activity under visible-light irradiation: the relationship between tunable optical absorption, defect chemistry and photocatalytic activity. *CrystEngComm*, 18, 1933-1943.
- [30] Zou, X.-H., Zhao, S.-W., Zhang, J.-G., Sun, H.-L., Pan, Q.-J., Guo, Y.-R. (2019). Preparation of ternary ZnO/Ag/cellulose and its enhanced photocatalytic degradation property on phenol and benzene in VOCs. *Open Chemistry*, 17, 779-787.
- [31] Vu, A.-T., Park, Y., Jeon, P.R., Lee, C.-H. (2014). Mesoporous MgO sorbent promoted with KNO<sub>3</sub> for CO<sub>2</sub> capture at intermediate temperatures. *Chem. Eng. J.*, 258, 254-264.
- [32] Park, J.H., Choppala, G., Lee, S.J., Bolan, N., Chung, J.W., Edraki, M. (2013). Comparative Sorption of Pb and Cd by Biochars and Its Implication for Metal Immobilization in Soils. *Water, Air, Soil Pollut.*, 224, 1711.

- [33] Vu, A.-T., Ho, K., Lee, C.-H. (2016). Removal of gaseous sulfur and phosphorus compounds by carbon-coated porous magnesium oxide composites. *Chem. Eng. J.*, 283, 1234-1243.
- [34] Bouzid, H., Faisal, M., Harraz, F.A., Al-Sayari, S.A., Ismail, A.A. (2015). Synthesis of mesoporous Ag/ZnO nanocrystals with enhanced photocatalytic activity. *Catal. Today*, 252, 20-26.
- [35] Kaur, A., Gupta, G., Ibhaddon, A.O., Salunke, D.B., Sinha, A.S.K., Kansal, S.K. (2018). A Facile synthesis of silver modified ZnO nanoplates for efficient removal of ofloxacin drug in aqueous phase under solar irradiation. *Journal of Environmental Chemical Engineering*, 6, 3621-3630.
- [36] Yang, X., Li, Y., Du, Q., Sun, J., Chen, L., Hu, S., Wang, Z., Xia, Y., Xia, L. (2015). Highly effective removal of basic fuchsin from aqueous solutions by anionic polyacrylamide/graphene oxide aerogels. *Journal of Colloid and Interface Science*, 453, 107-114.
- [37] Yang, C., Yu, J., Li, Q., Yu, Y. (2017). Facile synthesis of monodisperse porous ZnO nanospheres for organic pollutant degradation under simulated sunlight irradiation: The effect of operational parameters. *Mater. Res. Bull.*, 87, 72-83.
- [38] El-Sayed, G.O., Yehia, M.M., Asaad, A.A. (2014). Assessment of activated carbon prepared from corncob by chemical activation with phosphoric acid. *Water Resources and Industry*, 7-8, 66-75.
- [39] Yang, J.Y.C., Li, Q., Yu, Y. (2016). Facile synthesis of monodisperse porous ZnO nanospheres for organic pollutant degradation under simulated sunlight irradiation: The effect of operational parameters. *Materials Research Bulletin*, 87, 72-83.
- [40] Behnajady, N.M.M.A., Hamzavi, R. (2006). Kinetic study on photocatalytic degradation of C.I. Acid Yellow 23 by ZnO photocatalyst. *Journal of Hazardous Materials*, 133, 226-232.
- [41] Zyoud, A.Z.B.A., Helal, M.H.S., Park, D., Campet, G., Hilal, H.S. (2015). Optimizing photo-mineralization of aqueous methyl orange by nano-ZnO catalyst under simulated natural conditions. *Journal of Environmental Health Science & Engineering*, 13, 46-55.
- [42] Abhilash, M.R., Akshatha, G., Srikantaswamy, S. (2019). Photocatalytic dye degradation and biological activities of the Fe<sub>2</sub>O<sub>3</sub>/Cu<sub>2</sub>O nanocomposite. *RSC Advances*, 9, 8557-8568.
- [43] Ghiasi, E., Malekzadeh, A. (2020). Removal of Various Textile Dyes Using LaMn(Fe)O<sub>3</sub> and LaFeMn<sub>0.5</sub>O<sub>3</sub> Nanoperovskites; RSM Optimization, Isotherms and Kinetics Studies. *Journal of Inorganic and Organometallic Polymers and Materials*, 8, 1-16.
- [44] Zhang, Y.Z.H., Zhang, D.B. (2007). Decolorization and mineralization of CI Reactive Black 8 by Fenton and ultrasound/Fenton method. *Color. Techno.*, 123, 101-105.